OPEN

Correspondence and
requests for materials
should be addressed to
Y.-C.T. (yctai@mems.
caltech.edu) or S.-Y.Z.
(siyang@psu.edu)

* These authors
contributed equally to
this work.

Separable Bilayer Microfiltration Device for Viable Label-free Enrichment of Circulating Tumour Cells

Ming-Da Zhou[1]*, Sijie Hao[1]*, Anthony J. Williams[2,3,5]*, Ramdane A. Harouaka[1], Brett Schrand[3,4], Siddarth Rawal[2,5], Zheng Ao[2,3,5], Randall Brenneman[3,4], Eli Gilboa[4], Bo Lu[6], Shuwen Wang[7], Jiyue Zhu[7], Ram Datar[2,5], Richard Cote[2,5], Yu-Chong Tai[6] & Si-Yang Zheng[1]

[1]Micro & Nano Integrated Biosystem (MINIBio) Laboratory, Department of Biomedical Engineering and Materials Research Institute, Pennsylvania State University, University Park, PA 16802, U.S.A., [2]Department of Pathology, University of Miami – Miller School of Medicine, Miami, FL 33136, U.S.A., [3]Sheila and David Fuente Graduate Program in Cancer Biology, University of Miami – Miller School of Medicine, Miami, FL 33136, U.S.A., [4]Department of Microbiology and Immunology, University of Miami – Miller School of Medicine, Miami, FL 33136, U.S.A., [5]Dr John T Macdonald Foundation Biomedical Nanotechnology Institute, University of Miami – Miller School of Medicine, Miami, FL 33136, U.S.A., [6]Caltech Micromachining Laboratory, California Institute of Technology, MC 136-93, Pasadena, CA 91125, U.S.A., [7]Department of Pharmaceutical Sciences, Washington State University College of Pharmacy, Spokane, WA 99210, U.S.A.

The analysis of circulating tumour cells (CTCs) in cancer patients could provide important information for therapeutic management. Enrichment of *viable* CTCs could permit performance of functional analyses on CTCs to broaden understanding of metastatic disease. However, this has not been widely accomplished. Addressing this challenge, we present a separable bilayer (SB) microfilter for viable size-based CTC capture. Unlike other single-layer CTC microfilters, the precise gap between the two layers and the architecture of pore alignment result in drastic reduction in mechanical stress on CTCs, capturing them viably. Using multiple cancer cell lines spiked in healthy donor blood, the SB microfilter demonstrated high capture efficiency (78–83%), high retention of cell viability (71–74%), high tumour cell enrichment against leukocytes ($1.7–2 \times 10^3$), and widespread ability to establish cultures post-capture (100% of cell lines tested). In a metastatic mouse model, SB microfilters successfully enriched viable mouse CTCs from 0.4–0.6 mL whole mouse blood samples and established *in vitro* cultures for further genetic and functional analysis. Our preliminary studies reflect the efficacy of the SB microfilter device to efficiently and reliably enrich viable CTCs in animal model studies, constituting an exciting technology for new insights in cancer research.

M etastatic disease represents the ability of solid tumour cells to intravasate from their site of origin, travel through the haematogenous and/or lymphatic circulatory systems and extravasate at distant secondary sites where new tumours are colonized. In contrast to early stage disease, treatment strategies in the metastatic setting are largely palliative rather than curable, where over 90% of cancer-related mortality can be attributed to disease outgrowth beyond the primary site[1]. To improve the survival rates among late stage and recurrent cancer patients, 1) enhanced diagnostic tools for earlier detection, 2) treatment monitoring strategies that detect the underlying cellular and molecular changes arising from selective pressure posed by the treatment process, and 3) therapies that better target the metastatic cells directly are in urgent need.

Numerous studies suggest circulating tumour cells (CTCs), the tumour subpopulation responsible for invasion and colonization of distant sites, to be a candidate biomarker for prognosis, diagnosis and treatment monitoring of metastatic disease[2–5]. Assaying for CTCs requires only a simple, minimally invasive blood draw, providing a unique opportunity for repeated sampling in patients to monitor both metastatic disease as well as therapeutic response in real-time. Although promising for their diagnostic and prognostic potential, detecting and analysing CTCs is thwarted by their paucity, with only a few tumour cells occurring among billions of non-tumour cells in peripheral blood[4,6]. Thus highly efficient enrichment strategies are a prerequisite and a technical limitation for CTC analysis[7].

In recent years, a number of CTC enrichment systems have been developed[8,9]. Immunological approaches depend on cell surface antigen expression[10–12]. Epithelial cell surface markers expressed predominantly on CTCs, such as epithelial cell adhesion molecule (EpCAM), are widely used[13–23]. The CellSearch® system represents the
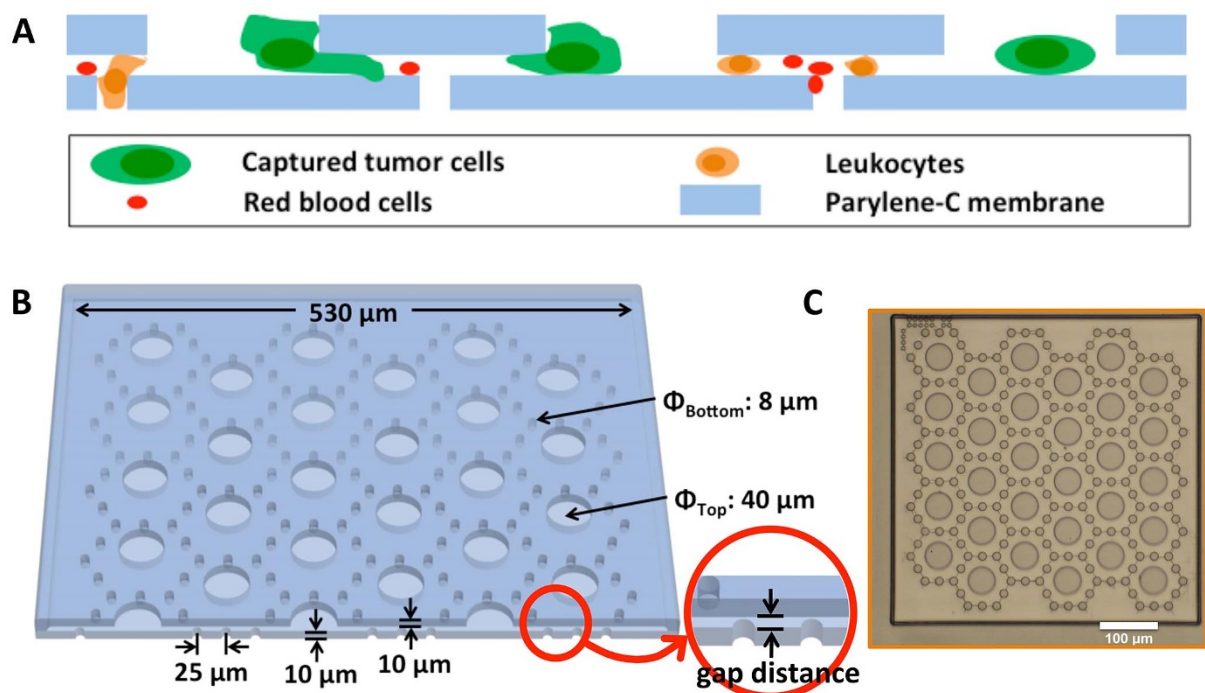
Figure 1 | Device design. (A): Cartoon of device cross-sectional view showing tumour cells are captured along the edges of the large top parylene-C pores; (B): 3D view of an elemental unit model with key geometrical parameters labelled, including the gap distance in inset; (C): Microscopic picture of top view of an elemental unit showing large pores on top parylene-C layer and small pores on bottom parylene-C layer with index dots on the top left corner. Scale bar is 100 μm.

most prominently used platform by this approached, which enriches CTCs from whole blood using an EpCAM-based immunomagnetic separation process[24–26]. Currently, it is the only FDA cleared clinical CTC analysis system for metastatic breast, prostate and colorectal cancers. In addition to immunological approaches, unique physical properties of cancer cells have also been exploited for CTC enrichment, including cell size, deformability, electrical and acoustic properties[18,27–31].

Beyond the enumeration and molecular characterization of CTCs, the development of the enrichment of viable CTCs enables their functional characterization that are critical for disease interrogation and target therapy[32–34]. Viable CTCs in metastatic breast cancer have been enriched using multi-marker FACS technology, where in one study a metastasis-initiating subpopulation of primary luminal breast cancer CTCs were used to generate a mouse xenograft model that gives rise to bone, lung and brain metastases[29]. In another study, a microfluidic device combined live CTC capture and "on-chip" treatment with taxol drugs to demonstrate microtubule organization alterations in CTCs[35].

Our group has previously described the development of a *2D round pore-shaped microfilter* fabricated on a single 10 μm-thick parylene-C membrane by photolithography[36]. Pre-fixation of blood samples are needed to prevent cell lysis during filtration, which makes it unusable for viable CTC enrichment. To alleviate this limitation, we developed a *3D membrane microfilter*, where blood samples are processed for CTC enrichment with no prior fixation[37]. While we demonstrated an ability to capture viable tumor cells in model systems, trapping of cells inside of the pores restricts cell proliferation and cell release.

Herein, we report the new design of a separable bilayer (SB) microfilter. The SB microfilter has fundamentally different device structure and filtration principles. These improvements have significantly enhanced our ability to enrich and characterize viable CTCs. We evaluated the performance of the SB microfilter device using both *in vitro* and *in vivo* systems, where we demonstrate (1) high sensitiv-

ity and efficiency of viable tumour cell capture, (2) the ability to enrich tumour cells from multiple types of cancer cell lines for their proliferation directly on the surface of the microfilter or on secondary culture surfaces, (3) the ability to enrich viable CTCs in a breast cancer mouse model system for subsequent cell culture and functional characterization, and (4) the ability to enrich viable CTCs from a clinical blood sample. The SB microfilter is a new, high performance viable CTC enrichment device with the potential to have important utility in both research and clinical applications.

Results

Design and operation of the SB microfilter. In the SB microfilter, the capture is realized by the gap between the top and bottom porous membranes (Figure 1A). They were made from biocompatible polymer parylene-C aiming to better preserve the viability of the cells. A 3D view in Figure 1B summarizes the geometrical design parameters. The bottom layer contains the 8 μm diameter holes arranged hexagonally. Larger holes of 40 μm diameter were created on the top parylene-C layer and aligned to the centres of the corresponding hexagon patterns on the bottom layer. An example elemental unit after fabrication is shown in Figure 1C. Each elemental unit is encoded by dots at the top left corner of the unit on the bottom parylene-C layer as an index to facilitate the identification and positioning of captured cells of interest.

The operation of the SB microfilter was first demonstrated using healthy blood samples spiked with tumour cell line. GFP expressing MCF-7 cells (green fluorescent) were spiked in whole blood and passed through the SB microfilter. An example of the microfilter following filtration is shown in Figure 2A&B. The majority of the captured tumour cells were located along the edges of the large top pores, although tumour cells could partially or completely wedge into the gap between the top and bottom parylene-C layers.

After the tumour cells are captured on the SB microfilters, it is possible to separate the top and bottom parylene-C membranes to access the captured cells. Figure 2C shows the concept and
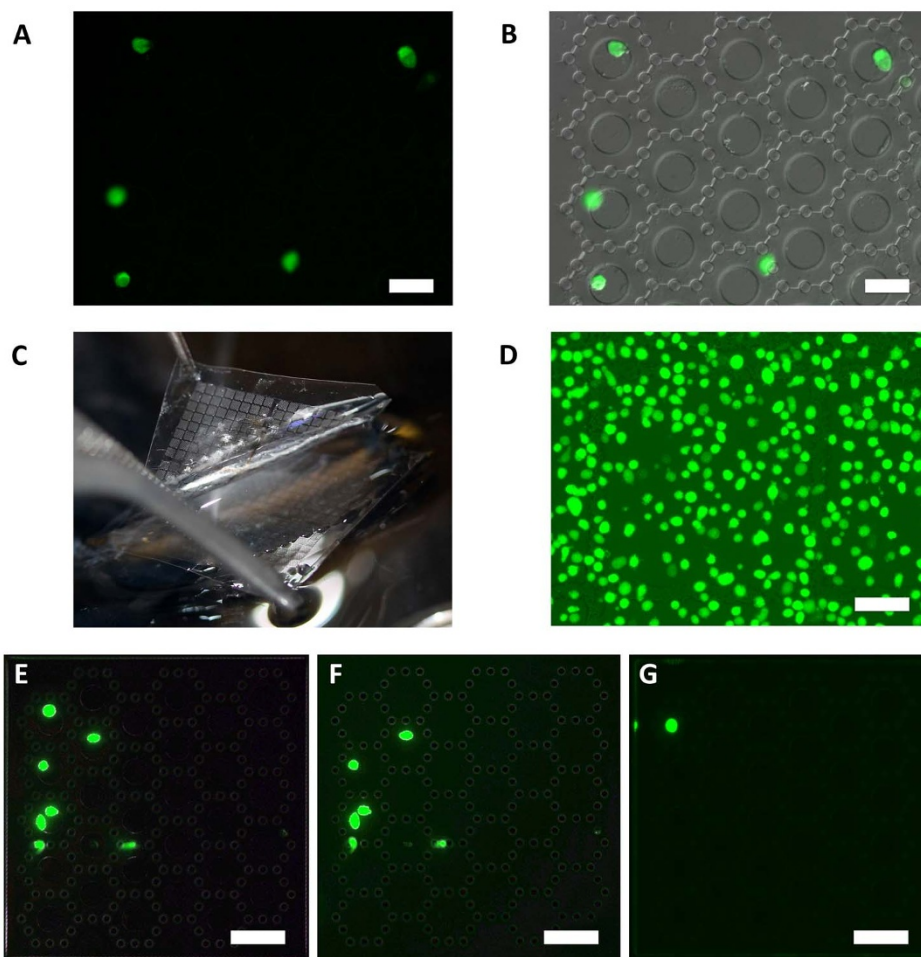
Figure 2 | Demonstration of the operation of the SB microfilter. (A)–(B): Representative areas of the SB microfilter after filtration. MCF-7 breast cancer cells were GFP-expressing (A) while surrounding blood cells could also be seen in bright field/fluorescence composite view (B). Scale bars are 50 μm. (C)–(G): The top and bottom parylene-C membrane layers can be separated after cell enrichment. (C): Image showing the concept of separable microfilter. (D): MDA-MB-231 cells labelled with CFDA-SE. (E): Cells captured on SB microfilter before separation of the top and bottom parylene-C layers. (F): The bottom parylene-C layer after separation. (G): The top parylene-C layer after separation. Scale bars are 100 μm.

Figure 2D–2G demonstrates an example using MDA-MB-231 cells labelled with long-term fluorescence cell tracer carboxyfluorescein diacetate, succinimidyl ester (CFDA-SE, Invitrogen CA). After cell capture, two pairs of tweezers were used to hold the edges of the top and bottom parylene-C membrane respectively. With minimal force, the two layers could be separated. The separable feature of the device is controlled by engineering the adhesion strength between the top and bottom parylene-C layers during microfabrication. In Figure 2E–2G, the majority of captured cells were maintained on the bottom parylene-C layer at their original positions after the separation of the two parylene-C membranes. Uncompromised green fluorescent intensity of the captured cells indicated that the cell viability was preserved during the separation.

Characterization of the SB microfilter. There are multiple performance parameters for CTC enrichment, including capture efficiency, enrichment, cell viability, blood sample capacity and processing speed. Often, some of these parameters are inversely related to each other. As a result, optimization requires achieving a compromise depending on specific downstream applications. The SB microfilter was tested with tumour cell lines spiked in DPBS, healthy human blood, blood from animal cancer models, and clinical blood samples.

The capture efficiency and enrichment were measured using two breast cancer cell lines: MCF-7, estrogen receptor and progesterone receptor (ER/PR) positive and less invasive; and MDA-MB-231, triple negative and highly invasive. The measured capture efficiencies were 83 ± 3% for MCF-7 and 78 ± 4% for MDA-MB-231 (n = 4 each) when ~130 cells in ~1 μL of DPBS were spiked in 1 mL of DPBS (Figure 3A). Assuming perfect capture efficiency, enrichment can be uncoupled from capture efficiency and measured independently[38]. The enrichment was thus determined by the retention of non-tumour leukocytes. The ratio of leukocytes inside the original blood sample and those left on the device was used as measured enrichment against leukocytes. The measured enrichment factors were $2.0 \pm 0.3 \times 10^3$ for MCF-7 and $1.7 \pm 0.4 \times 10^3$ for MDA-MB-231 (Figure 3B). The measured capture efficiency and enrichment factors are comparable to the previous 3D microfilters with similar double layer membrane structure[37].

Cell viability after captured on SB microfilters. An important feature of the SB microfilter is its capability for viable cell enrichment. In contrast to the 2D pore-shaped microfilter, the SB microfilter is capable of processing unfixed and undiluted whole blood samples. This not only eliminates sample manipulation steps before filtration, but more importantly enables downstream applications that require the viability of cells. Two approaches were employed to study cell viability after enrichment. First, the viability of MCF-7 and MDA-MB-231 cancer cells after filtration were determined with the LIVE/DEAD viability assay using
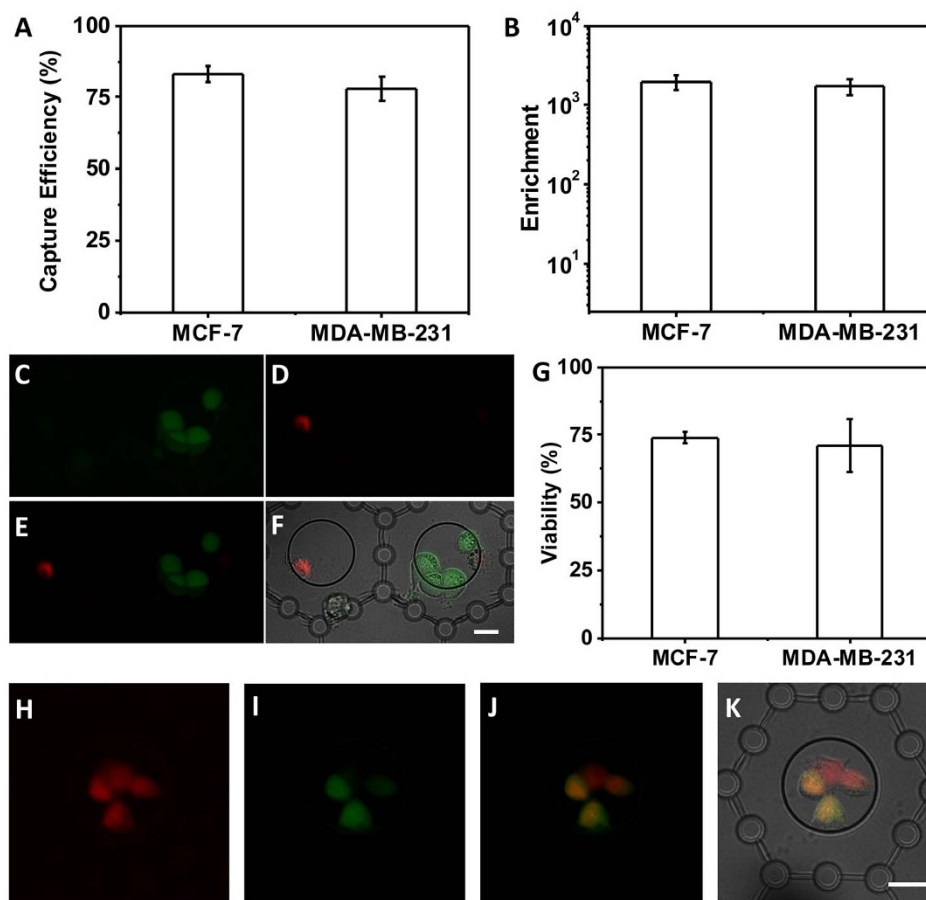
Figure 3 | **Characterization of device performance.** (A): Capture efficiency is measured and plotted for two cell lines, MCF-7 and MDA-MB-231 human breast cancer cell lines. Each column shows the mean value and its standard deviation (n = 4). (B): Enrichment factor from undiluted human blood is measured and plotted. Each column shows the mean value and its standard deviation (n = 4). (C)–(G): LIVE/DEAD assay with representative areas of the SB microfilter after filtration. Viable MDA-MB-231 cancer cells are highlighted with green (C) while dead tumour cells are in red (D). Fluorescence composite (E) and differential interference contrast (DIC)/fluorescence composite (F) of tumour cells detected in A and B. LIVE/DEAD cell assay consisting of viable cell indicator Calcein-AM green and the exclusion dye Ethidium Homodimer-1 were used. (G): Cell viability after filtration is measured and plotted for two cell lines, MCF-7 and MDA-MB-231 human breast cancer cell lines. Each column shows the mean value and its standard deviation (n = 4). (H)–(K): Cell viability detected by virus infection. The mCherry-expressing MCF-7 cells were used. Infected viable cancer cells expressed green fluorescence protein. The captured MCF-7 cancer cells were highlighted with red (H) while infected viable tumour cells were in green (I). Fluorescence composite image (J) and differential interference contrast (DIC) image overlaid with fluorescence composite image (K) of tumour cells detected in (A) and (B). Scale bars are 10 μm.

Calcein-AM green and Ethidium Homodimer-1 (EthD-1). Calcein-AM green is a permeable fluorogenic esterase substrate that reacts with cells containing active enzyme activity, thus labelling viable cells with green fluorescence, while impermeable DNA binding dye EthD-1 only reaches the nucleus when the plasma membrane has been compromised or destroyed, thus labelling dead cells with red fluorescence. An example of such on-chip LIVE/DEAD analysis is shown in Figure 3C–3F. Cell viability is defined as the ratio of live cells versus total cells on the microfilter after the filtration. Each assay was repeated four times for each cell line. The calculated cell viability was 74 ± 2% for MCF-7 and 71 ± 9% for MDA-MB-231 cancer cells (Figure 3G). As a control, the viability assay was also performed on tumour cells that weren't passed through the SB microfilter. Instead of using the microfilter, cell counting was carried out on a glass microscope slide. The calculated viability was 95 ± 3% from triplicate control samples (data not shown).

In the second approach to demonstrate cell viability after filtration, wild adenovirus type 5 was modified with green fluorescence expression gene eGFP under the control of CMV promoter. It has been shown that modified adenovirus can preferably infect and express in tumour cells and thus can be used as a tool for viable CTC detection[39]. In this experiment, MCF-7 cells were modified with a red fluorescence expressing mCherry gene. As shown in Figure 4H–4K, cells with both red and green fluorescence (mCherry⁺GFP⁺) represented virus-infected viable MCF-7 cells, while cells with only red fluorescence (mCherry⁺GFP⁻) are presumably non-viable cells. The virus infection assay probed the cell's ability to actively express proteins (GFP in this case). Therefore, it is a different viability indicator compared with the measurement of membrane permeability (EthD-1) and enzyme activity (Calcein-AM). It should be noted that, assigning all the mCherry⁺GFP⁻ as non-viable tumour cells made an assumption that the efficiency of virus infection and GFP expression in viable tumour cells was 100%. Based on the initial test, the virus infection efficiency was measured to be 90% ∼ 95% depending on the tumour cell lines (data not shown).

Cell proliferation following capture by the SB microfilters. To investigate whether captured tumour cells can proliferate directly on the SB microfilters, tumour cells from various cell lines (DU145, Hela, LnCaP and PC3) were spiked in DPBS and captured on SB microfilters, respectively. The SB microfilters were placed individually in a six-well plate and cultured as using standard
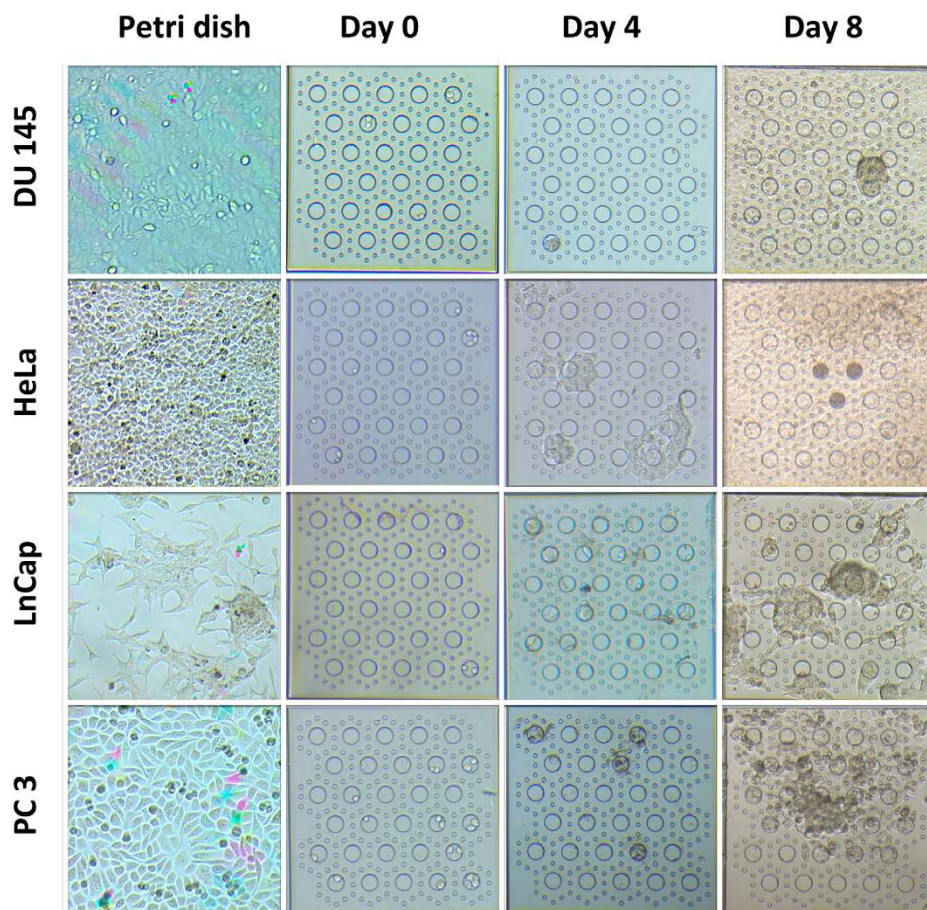
Figure 4 | On-chip cell proliferation demonstrated with various cell lines (DU145, Hela, LnCaP and PC3). The images in each column are bright field microscopic images of cell growth on Petri dish as positive control and day 0, 4, and 8 on SB microfilters after enrichment.

conditions of the particular cell lines. As shown in Figure 4, captured tumour cells grew into colonies on day 4 following filtration and large patches of confluency were observed by day 8. The morphology of cells and the shape of colonies shared similarity with that of the parental cells growing under the standard conditions. It is encouraging to observe that following SB microfilter enrichment, captured tumour cells can proliferate directly on-chip, a critical step forward towards CTC culture from clinical blood samples.

Demonstration of SB microfilter performance in mouse model systems. Primary tumours were established in 100% (6/6) of mice injected, and in vitro cell cultures from each primary tumour digested were successfully established in all cases. Cell cultures were established from blood samples in 33% (1/3) of mice injected with 4T1 and 4T07 cells, respectively, demonstrating SB microfilter's ability to permit tumour cell expansion directly on-chip (Figure 5A). An advantage of this *in vivo* mouse model system is that 4T1 and 4T07 tumour cells are resistant to treatment with 6-Thioguanine (6-TG)[40]. Thus, to confirm whether cells captured by the SB microfilter device originated from their primary tumours, viable cells were mechanically released by physical separation of the SB microfilter layers, placed in 96-well plates in triplicate, and grown in the presence of RPMI culture media supplemented with 50 mM 6-TG (Sigma-Aldrich, St Louis MO) for 5 days. After drug treatment, cell viability was assessed using the CellTiter Blue assay (Promega, Madison WI) where viable cells reduce resazurin to resourufin, which produces a fluorescent signal that can be detected by a plate reader at 590 nm. In contrast to SKBR-3 breast cancer cells that demonstrate sensitivity to 6-TG treatment, primary tumours and corresponding CTCs from 4T1 and 4T07 cells show similar

viability in the presence of 6-TG compared to untreated controls (Figure 5B). Further, the execution of this experiment demonstrates the ability to release cells from the SB microfilter with efficiency and successfully culture tumour cells on surfaces other than the parylene-C membrane.

After establishing that our device captured CTCs that originated from 4T1 and 4T07 primary tumours, we injected 1×10^4 4T1 CTCs, 4T07 CTCs, and their respective corresponding parental cell lines as positive controls, into the mammary fat pad (FP; n = 5 each) of BALB/C mice. Tumours were allowed to form in all groups injected FP for 20 days, when they were sacrificed, primary tumour was removed and prepared for histological analysis as described above. As shown in Figure 5C, tumours were established in 100% (20/20) of mice with no discernable differences in the tumour volume and rate of growth between viable CTCs recovered by the SB microfilter device and that of their corresponding parental cell lines (data not shown), demonstrating similar tumourigenicity. Further studies on the mouse CTCs derived animal models are currently underway, and will be reported separately.

In our studies, 0.4–0.6 mL whole mouse blood was drawn from each mouse by submandibular cheek puncture for viable CTC enrichment. Using the same procedure, the SB microfilter can enrich CTCs from ~0.1 mL whole mouse blood, which is a safe blood volume that can be drawn from adult mice repetitively (e.g. weekly). This will enable CTC studies in mouse models of metastasis, which is critically important to improve our current understanding of the overall metastatic process.

Clinical sample testing with SB microfilter. We investigated the feasibility of using the current 1 cm² SB microfilter for CTC
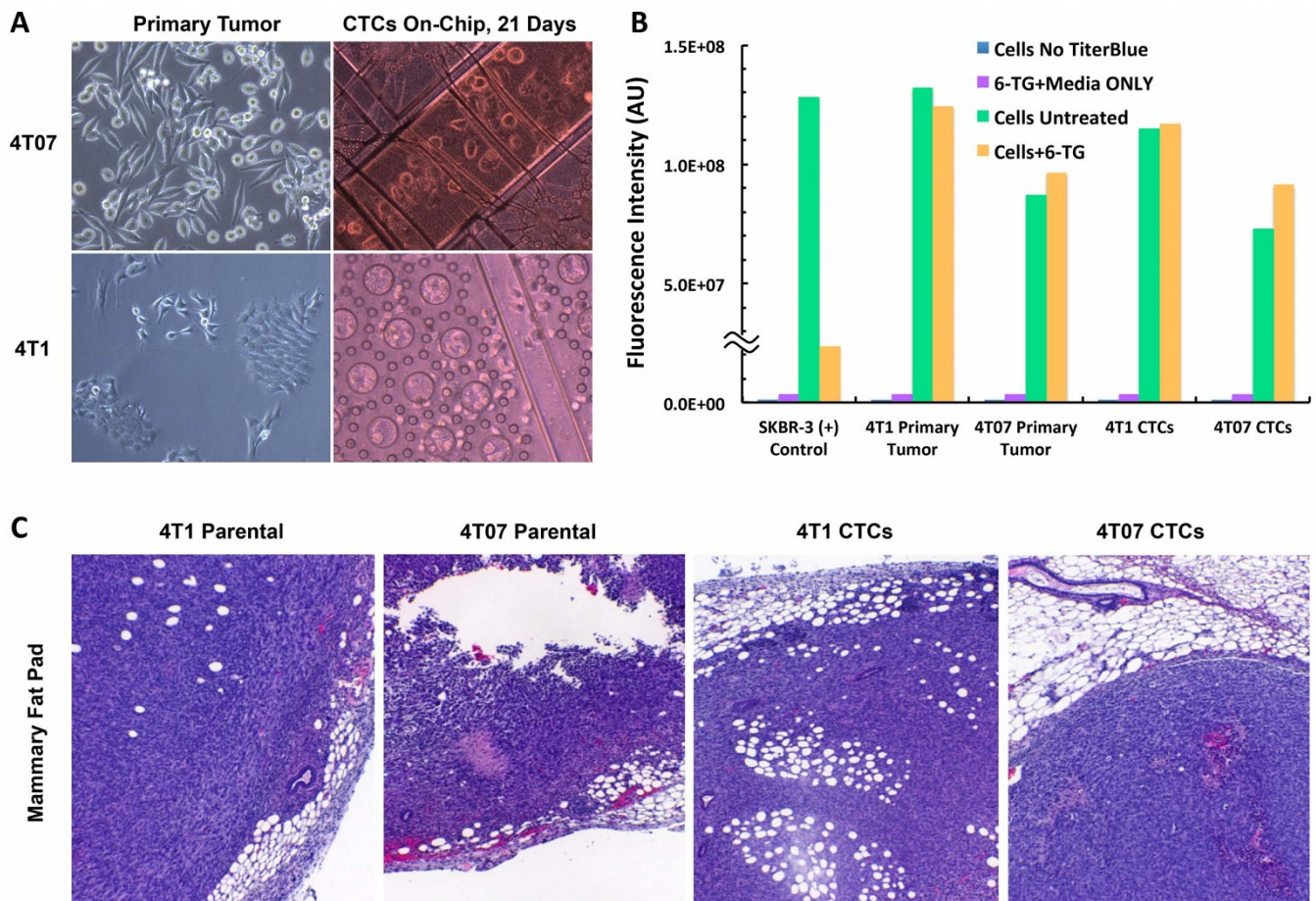
Figure 5 | In vivo study of tumourigenicity of 4T1 and 4T07 CTCs in mouse models. (A): 4T07 and 4T1 viable CTCs captured by the bilayer microfilter device on-chip 21 days after their enrichment from whole blood, and their corresponding primary tumours in culture. In both tumour types, CTCs were found inside the central pore as well as around the central pore and in the margins of the bilayer membrane device, indicating their ability to migrate away from the original site capture. (B): Fluorescent intensities of primary tumour cells and viable CTCs cultured in the presence of 6-TG treatment (orange) compared to untreated controls (green). The fluorescent intensities of tumour cells with no TiterBlue reagent (blue) and 6-TG + culture media alone (purple) were also measured as a control, and demonstrate that there was no auto fluorescence contributing to the signals detected in treated versus untreated samples. (AU = Arbitrary Units). (C): H&E staining of FFPE sections from viable 4T1 and 4T07 CTCs captured by the SB microfilter. CTCs injected into mammary fads of mice demonstrate the formation of poorly differentiated, invasive tumours characteristically similar to their corresponding parental cell lines.

enrichment from clinical blood samples. One mL whole blood from each metastatic colorectal cancer patients was applied to the device. After enrichment, on-chip cocktail immunocytochemical staining for CK 8/18/19 (red), CD-45 (green, pseudo-colour) and DAPI (blue) were used to positively and negatively select CTCs and non-tumour, nucleated blood cells, respectively. One example is shown in Supplementary data (Figure S1), where a CTC (CK$^+$/CD45$^-$/DAPI$^+$) was captured and detected on the edge of the pore on top parylene-C membrane, while smaller leukocytes (CK$^-$/CD45$^+$/DAPI$^+$) were trapped between the top and bottom parylene-C layers. For a 1 cm^2 device, the practical blood sample capacity was limited to ~1.5 mL. It is worth noting that, while the current SB microfilter device is capable of processing a whole tube of fresh blood of 7.5 mL, it takes much longer and has a higher risk of clogging the device (Supplementary data, Figures S2 and S3). Also for 7.5 mL whole blood, the captured cells are too crowded to maintain cancer cell morphology, which might prevent further analysis.

Discussion

One challenge of cell surface antigen dependent CTC enrichment is that CTCs in clinical blood samples are highly heterogeneous in surface antigen expression, and the EpCAM-based approach only selects for CTC subpopulations with high EpCAM expression. Further, EpCAM expression is absent from ~15–30% solid tumours and down-regulated in many CTCs, especially those believed to have undergone epithelial-mesenchymal transition (EMT) or those harbouring stem/progenitor phenotypes[41–44]. Independent of surface antigen expression, size-based enrichment is a particularly attractive approach based on the observation that malignant tumour cells are characteristically larger and less deformable than most of the non-tumour blood cell counterparts[45,46]. Importantly, this allows the potential to isolate a more heterogeneous population of CTCs. Caution should be exercised in this approach, as with any other enrichment methods, since small CTCs in clinical samples their significance are still under investigation[17].

Previously we designed various microfabricated filtration devices for size-based CTC enrichment applications. One of the most recent viable CTC enrichment devices, the 3D microfilter, has two layers of integrated parylene-C membranes, with 9 and 8 μm diameter una-ligned pores on the top and bottom parylene-C membranes, respectively[37]. Tumour cells are larger than blood cells and captured inside the top pore, while blood cells can penetrate the top pores, gaps between the top and bottom membranes and then the bottom pores. The device was demonstrated to capture viable tumour cells.
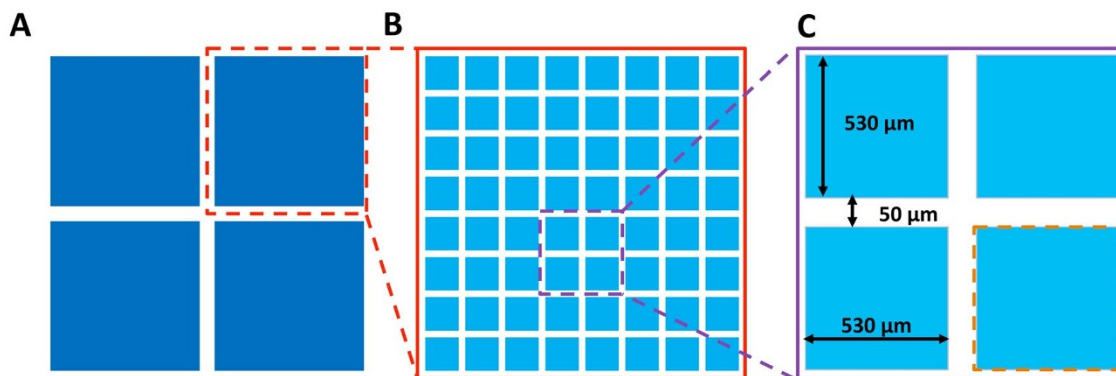
Figure 6 | Device design. (A): Each device has four large filter patches; (B): Each filter patch is an 8 by 8 array of elemental units; (C): Geometry of four elemental units and their arrangement. A picture of an elemental unit (boxed in orange dash lines) is shown in Figure 1C.

However, cells did not proliferate presumably due to the limited space provided by the top pores (9 μm diameter) where cells were captured and immobilized tightly without extra space.

In this study, we designed, microfabricated and characterized a new three-dimensional microfilter for viable CTC enrichment based on physical properties of the cells. Compared with the fabrication process of the previous 3D microfilter[37], there are several major changes and the overall process has a much higher yield. First, the SB microfilter was completely constructed with parylene-C, a transparent and biocompatible polymer, without a silicon support as the 3D microfilter. Although the device is still made on silicon substrate, the wafer is only served as a device carrier. As a result, the SB device fabrication process eliminates the demanding fabrication steps of double side alignment and through wafer etching as in the 3D microfilter. Secondly, the pores on the top parylene layer have a large diameter of 40 μm, thus CTCs are not captured inside the top pores on the SB microfilter, but instead trapped in the gaps at the edge of large top pores and the bottom parylene-C layer. This design specification allows greater freedom for enriched tumour cells to expand, migrate, and proliferate on the surface of the device. The key fabrication parameter to be controlled during fabrication is the thickness of the sacrificial photoresist, which determines the gap distance between the top and bottom parylene-C membranes and can be controlled down to ~0.1 μm resolution. Another important design characteristic of the SB microfilter is that the adhesion between the top and bottom parylene layers are controlled during microfabrication to make it strong enough to hold in-place during operation, but they can be separated easily with tweezers afterwards. The exposed cells are thus more accessible to chemicals that for

examples disrupt cell adhesion for more efficient release, stain cells for imaging or lyse cells for genetic analysis. The critical innovations we have made to our multilayer technology enabled us to extend the fundamental working principles and advantages of size-based CTC enrichment to viable cell capture and functional characterization.

We demonstrated the viability and proliferative capacity of captured cells by the SB microfilter using multiple cancer cell lines *in vitro*. The efficacy of the SB microfilter device was further validated using whole blood samples from a breast cancer mouse model system *in vivo*, demonstrating our ability to capture and culture viable CTCs from mice injected with tumour cells of varying metastatic capacity. The SB microfilter succeeded in enrichment and *in vitro* culture of CTCs from hundreds of microliters of mouse blood. Considering the current 1 cm² SB microfilter process whole blood volume in the range of 0.1–1.5 mL, which perfectly fit the total bleed out volume for adult mouse of 0.6–1.4 mL[47], thus this device is a highly valuable tool for CTC studies in pre-clinical mouse models.

In a feasibility study, the SB microfilter was shown to capture CTCs from an unfixed metastatic cancer patient blood sample. Since it is desirable to assess larger blood volumes (e.g. a full tube of blood of 7.5 mL) in a clinical setting, future study will increase sample-processing capacity by expanding the effective filtration area. Further, the maintenance of CTC cultures from human blood samples is a more complicated task than in mouse model systems. However, recent report on CTC culture after enrichment by CTC-iChip demonstrated the feasibility[48]. In addition to viable CTC isolation, the optimal culture conditions for CTC expansion will need to be determined. An important advantage of the SB microfilter is its ability to simultaneously act as a capture, analysis, and culture plat-
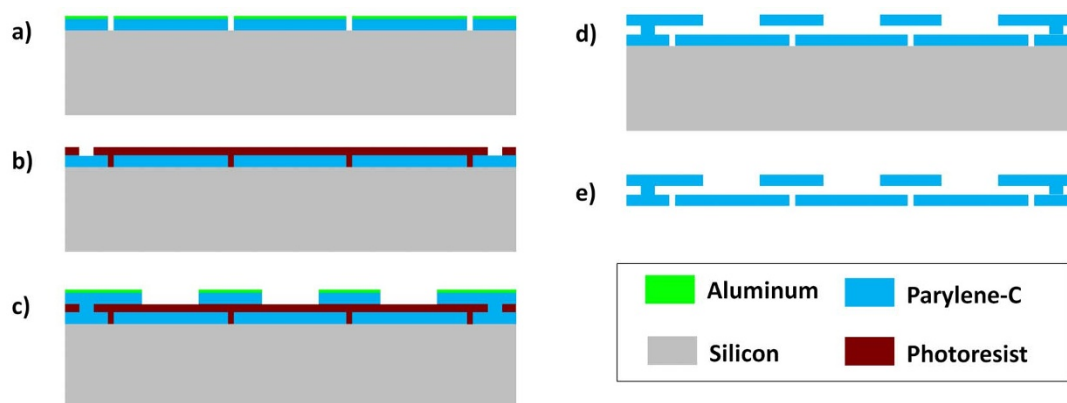
Figure 7 | Process flow of SB microfilter device fabrication. (a) Deposition and patterning of bottom layer parylene-C; (b) Patterning of sacrificial photoresist; (c) Deposition and patterning of top layer parylene-C; (d) Removal of residual aluminum film and sacrificial photoresist; (e) Release of device from the substrate.

Figure 8 | Filtration setup including device housing.

form, which can easily be integrated with highly efficient next-generation culture reagents[49–51] in the future aiming at expanding tumour cells *in vitro* from low numbers of founder cells.

Our technology provides the opportunity to perform functional characterization of CTC beyond their enumeration, a critical step towards a better understanding of the mechanisms underlying CTC release, haematogenous spread, and colonization of distant sites. Such studies will be critical in elucidating functionally important tumour cell subsets and tumorigenic CTCs for improved patient management. The further development of technologies aimed at functional CTC characterization could have profound implications on the basic and translational study of cancer, such as the establishment of *in vivo* models for metastasis that more closely resemble disease while in transit to secondary sites. Further, the *in vitro* maintenance of viable CTC enriched from cancer patients could permit the development of drug sensitivity assays, such that an assessment can be made to predict whether a course of adjuvant therapy is suitable for a patient before treatment begins, monitor the efficacy of an on-going treatment in real-time, as well as potentially expose novel mechanisms for resistance to a given therapy. Our work could be the basis to reliably establish CTC cultures from human patients and provide a transformative approach to the functional characterization of CTCs, leading to exciting new avenues for improved patient management and cancer research.

Methods

Device design. A device is composed of a 2 by 2 array of filter patches (Figure 6A). Each patch is an 8 by 8 array of the elemental units (Figure 6B). Each elemental unit is 530 μm by 530 μm in dimension. An element unit is separated from its neighbours by 50 μm (Figure 6C). These 50 μm borders are where the top and bottom parylene-C layers adhere to each other. The gap between the top and bottom parylene-C membranes can be precisely defined (5.5 μm in the current device) by the thickness of the sacrificial photoresist. The bottom layer contains the 8 μm diameter holes arranged hexagonally. The centre-to-centre distance of the 8 μm diameter holes is

25 μm. Larger holes of 40 μm diameter are created on the top layer and aligned to the centres of the corresponding hexagon patterns on the bottom layer.

Fabrication process. Figure 7 illustrates the process flow of the device fabrication. It began with surface treatment of a single side 6-inch wafer with oxygen plasma. The first layer of 10 μm-thick parylene-C was deposited subsequently. A thin layer of aluminum was thermally evaporated and patterned with lithography and aluminum etchant type D. Parylene-C was etched with oxygen plasma with the aluminum as the mask. A 5.5 μm-thick SPR 955 photoresist was spin-coated after dissolving the aluminum mask with aluminum etchant. The photoresist was patterned with photolithography and serves as the sacrificial layer, which defined the gap between the top and the bottom parylene-C layers. A second layer of 10 μm-thick parylene-C was deposited. Prior to the deposition for the second layer of parylene-C, the exposed area of the first layer parylene-C was treated with oxygen plasma. Another layer of aluminum was thermally deposited and patterned with photolithography and aluminum etchant. The top parylene-C was patterned with oxygen plasma, after which the aluminum mask was dissolved again with aluminum etchant. The sacrificial photoresist was dissolved with acetone and rinsed with isopropyl alcohol and deionized water. Finally the device was released from the substrate.

Filtration assembly and process. After device fabrication, it was assembled into a device housing, which was similar to our previous reports[38,46]. During filtration the SB microfilter was secured between two sealing O-rings formed from polydimethylsiloxane (PDMS; DOW Corning) and clamped inside of a plastic housing cassette. The top piece of the housing cassette connected to a sample-loading syringe while the bottom piece of the housing cassette included a luer adapter for integration with a waste trap (Figure 8). This housing assembly acted as a reliable support for the SB microfilter and eliminates the possibility of fluid leakage. Blood samples were passed through the SB microfilter under gravity flow.

Cell culture. Human breast cancer cell lines MCF-7 and MDA-MB 231 were cultured in high glucose DMEM or RPMI-1640 base medium. LNCaP were cultured in RPMI-1640 culture medium. DU-145 and HeLa cells were cultured in EMEM culture medium. Human prostate cancer cell line PC-3 was cultured in F-12K culture medium. The base media were supplemented with 10% fetal bovine serum (FBS), 100 units/mL penicillin and 100 μg/mL streptomycin (Invitrogen, Carlsbad CA) in humidified incubators at 5% CO_2 and 37°C ambient temperature. At 70–80% confluency, cells were harvested from culture flasks by incubation with 0.25% Trypsin-EDTA (Invitrogen Carlsbad CA), washed in 1 × Dulbecco's phosphate buffered saline (1 × DPBS; Invitrogen, Carlsbad CA), and used for use in subsequent experiments described below.

Collection of blood samples. Healthy blood was obtained from consented donors at the Penn State General Clinical Research Centre according to an Institutional Review Board (IRB) approved protocol. Samples were drawn into EDTA-coated vacutainer tubes (Becton Dickinson, Franklin Lakes, NJ) from peripheral venepuncture. Blood samples were processed immediately upon receipt to facilitate optimal filtration conditions.

Capture efficiency measurement. Harvested MCF-7 and MDA-MB-231 breast cancer cells were incubated with acridine orange (Invitrogen Carlsbad CA) at room temperature for 5 minutes. The tumour cells were then washed three times in 1 × DPBS, placed on 96-well plates and counted. One μL of appropriately diluted tumour cells were spiked into 1 mL of undiluted healthy human blood and passed through the SB microfilter. After filtration the device was washed with 1 mL of DPBS. The SB microfilters were observed under a fluorescence microscope to determine the number of captured tumour cells.

Measurement of tumour cell enrichment against leukocytes. The enrichment factor is defined as the ratio of tumour cells to leukocytes left on the filter after filtration divided by that before filtration. Assuming perfect CTC capture efficiency, the enrichment can be simplified as the ratio of the number of leukocytes in the blood sample before filtration to the number of leukocytes remaining on the device after filtration. To measure enrichment, 1 mL of undiluted blood was passed through the SB microfilter with the same conditions described above for capture efficiency. The devices were washed with 1 × DPBS immediately after filtration and fixed with 4% paraformaldehyde (VWR) for 20 minutes. 1 μg/mL of 4′, 6-diamidino-2-phenylindole (DAPI; Invitrogen, Carlsbad CA) was used for nuclear visualization. The devices were observed under a fluorescence microscope and imaged at various locations on the device at 10 × magnification. A threshold was set based on fluorescence intensity. Acquired images were then processed using ImageJ (National Institute of Health, Bethesda MD) to enumerate nucleated cells.

Cell viability assay. MCF-7 and MDA-MB-231 breast cancer cells were diluted in 1 × DPBS on 96-well plates and counted. 150 cells were spiked into 1 mL of DPBS and passed through the SB microfilter. After filtration the devices were washed with 1 mL 1 × DPBS and stained with the LIVE/DEAD cell assay (Invitrogen, Carlsbad CA) where viable cells are reactive with Calcein-AM green (8 μM) and non-viable, apoptotic or dead cells are reactive with Ethidium Homodimer-1 (EthD-1, 4 μM). Captured cells were observed directly on the SB microfilter devices under a fluorescence microscope to determine the number of viable cells that were positive for Calcein-AM reactivity (green) and negative for Ethidium Homodimer-1 (red).

Virus infection assay for cell viability. The microfilters were washed with DPBS immediately after filtration and transferred into a 6-well plate containing 1.5 mL of DMEM medium. 100 μL DMEM medium was added to the top chamber formed between the sealing o-ring and the microfilters. The captured tumour cells were immediately infected with 10^7 pfu/mL recombinant adenoviruses Ad5GΔE3, where in wild-type adenoviruses the dispensable E3 gene was replaced with a CMV-eGFP expression cassette. Captured tumour cells were incubated for 24 hours in humidified incubators at 37°C with 5% CO_2 to allow virus infection and GFP expression.

Cell proliferability after enrichment. DU145, Hela, LnCaP and PC3 cells were appropriately diluted and spiked into DPBS with final concentration of ~10^3 per mL, respectively, and passed through the SB microfilter as described above. The SB microfilters were then transferred into different wells of a six-well plate and cultured directly on the surface of the device as described above.

In vivo animal model systems. Immunocompetent, Balb/C mice (n = 6) were injected into the mammary fat pad with 1×10^4 4T1 (n = 3) or 4T07 (n = 3) mouse mammary tumour cells possessing high metastatic and poor metastatic potential, respectively. Both mouse tumour cells lines are derived from the same spontaneously arising mammary tumour from Balb/cfC3H mice. At 25 days, the mice were sacrificed, and primary tumours were surgically resected. Half of each primary tumour was digested in 200 units/mL of collagenase IV (Invitrogen, Carlsbad CA) and placed into T75 flasks with RPMI at 37°C for culture, while the other half of primary tumours were fixed in 10% neutral buffered formalin for >24 hours and embedded in paraffin for immunohistochemical/immunofluorescent (IHC/IF) analyses. To confirm the presence of tumour growth in the mammary fat pad, 5 μm FFPE sections were prepared using a microtome, mounted onto glass microscope slides and baked overnight at 57°C. The tissue sections were then deparaffinized in xylene for 10 minutes, rehydrated with washes in decreasing concentrations of alcohol (100%, 90%, and 70%, for 5 minutes each), briefly rinsed with water, incubated in CAT Hematoxylin (Biocare Medical, Concord CA) for 4 minutes, briefly rinsed with water, incubated in Tacha's Bluing Solution (Biocare Medical, Concord CA), dipped 10 times in Eosin-Y (Richard Allan Scientific, Kalamazoo MI), dehydrated with washes in increasing concentrations of alcohol (70%, 90%, 100%, for 5 minutes each), incubated in xylene for 5 minutes, then coverslipped using mounting medium (Richard Allan Scientific, Kalamazoo MI). Approximately 0.4–0.6 mL whole blood was drawn from each mouse by submandibular cheek puncture into 1.5 mL Eppendorf tubes containing 25 units sodium heparin (Sigma-Aldrich, St Louis, MO) in HBSS. Whole blood samples were immediately diluted to a final volume of 5 mL in 1 × Hank's balanced salt solution (1 × HBSS; Invitrogen, Carlsbad CA) and processed by the SB microfilter device as described above. Successfully established tumour cell cultures from primary tumours and corresponding CTCs were further characterized by molecular and functional analyses.

1. Mehlen, P. & Puisieux, A. Metastasis: a question of life or death. *Nat Rev Cancer* **6**, 449–458 (2006).
2. Harouaka, R., Kang, Z., Zheng, S.-Y. & Cao, L. Circulating tumor cells: Advances in isolation and analysis, and challenges for clinical applications. *Pharmacology & Therapeutics* **141**, 209–221 (2014).
3. Pantel, K. & Alix-Panabieres, C. The clinical significance of circulating tumor cells. *Nat Clin Prac Oncol.* **4**, 62–63 (2007).
4. Pantel, K., Brakenhoff, R. H. & Brandt, B. Detection, clinical relevance and specific biological properties of disseminating tumour cells. *Nat Rev Cancer* **8**, 329–340 (2008).
5. Liberko, M., Kolostova, K. & Bobek, V. Essentials of circulating tumor cells for clinical research and practice. *Crit Rev Oncol Hematol* **88**, 338–356 (2013).
6. den Toonder, J. Circulating tumor cells: the Grand Challenge. *Lab Chip* **11**, 375–377 (2011).
7. Alix-Panabières, C., Schwarzenbach, H. & Pantel, K. Circulating Tumor Cells and Circulating Tumor DNA. *Annu Rev Med* **63**, 199–215 (2012).
8. Chen, J., Li, J. & Sun, Y. Microfluidic approaches for cancer cell detection, characterization, and separation. *Lab Chip* **12**, 1753–1767 (2012).
9. Arya, S. K., Lim, B. & Rahman, A. R. A. Enrichment, detection and clinical significance of circulating tumor cells. *Lab Chip* **13**, 1995–2027 (2013).
10. Lara, O., Tong, X. D., Zborowski, M. & Chalmers, J. J. Enrichment of rare cancer cells through depletion of normal cells using density and flow-through, immunomagnetic cell separation. *Exp Hematol* **32**, 891–904 (2004).
11. Hyun, K.-A., Lee, T. Y. & Jung, H.-I. Negative Enrichment of Circulating Tumor Cells Using a Geometrically Activated Surface Interaction Chip. *Anal Chem* **85**, 4439–4445 (2013).
12. Yang, L. et al. Optimization of an enrichment process for circulating tumor cells from the blood of head and neck cancer patients through depletion of normal cells. *Biotechnol Bioeng* **102**, 521–534 (2009).
13. Huang, Y.-y. et al. Immunomagnetic nanoscreening of circulating tumor cells with a motion controlled microfluidic system. *Biomed Microdevices* **15**, 673–681 (2013).
14. Li, P., Stratton, Z. S., Dao, M., Ritz, J. & Huang, T. J. Probing circulating tumor cells in microfluidics. *Lab Chip* **13**, 602–609 (2013).
15. Wang, L., Asghar, W., Demirci, U. & Wan, Y. Nanostructured substrates for isolation of circulating tumor cells. *Nano Today* **8**, 374–387 (2013).
16. Zhang, N. et al. Electrospun TiO2 Nanofiber-Based Cell Capture Assay for Detecting Circulating Tumor Cells from Colorectal and Gastric Cancer Patients. *Adv Mater* **24**, 2756–2760 (2012).
17. Stott, S. L. et al. Isolation of circulating tumor cells using a microvortex-generating herringbone-chip. *Proc Natl Acad Sci* **107**, 18392–18397 (2010).
18. Ozkumur, E. et al. Inertial Focusing for Tumor Antigen–Dependent and –Independent Sorting of Rare Circulating Tumor Cells. *Sci Transl Med* **5**, 179ra147, 1–11 (2013).
19. Nagrath, S. et al. Isolation of rare circulating tumour cells in cancer patients by microchip technology. *Nature* **450**, 1235–1239 (2007).
20. Yu, M. et al. Circulating Breast Tumor Cells Exhibit Dynamic Changes in Epithelial and Mesenchymal Composition. *Science* **339**, 580–584 (2013).
21. Stott, S. L. et al. Isolation and Characterization of Circulating Tumor Cells from Patients with Localized and Metastatic Prostate Cancer. *Sci Transl Med* **2**, 25ra23, 1–10 (2010).
22. Maheswaran, S. et al. Detection of mutations in EGFR in circulating lung-cancer cells. *NEJM* **359**, 366–377 (2008).
23. Gach, P. C., Attayek, P. J., Whittlesey, R. L., Yeh, J. J. & Allbritton, N. L. Micropallet arrays for the capture, isolation and culture of circulating tumor cells from whole blood of mice engrafted with primary human pancreatic adenocarcinoma. *Biosens Bioelectron* **54**, 476–483 (2014).
24. Shaffer, D. R. et al. Circulating Tumor Cell Analysis in Patients with Progressive Castration-Resistant Prostate Cancer. *Clin Cancer Res* **13**, 2023–2029 (2007).
25. Cristofanilli, M. et al. Circulating Tumor Cells, Disease Progression, and Survival in Metastatic Breast Cancer. *NEJM* **351**, 781–791 (2004).
26. Cohen, S. J. et al. Relationship of Circulating Tumor Cells to Tumor Response, Progression-Free Survival, and Overall Survival in Patients With Metastatic Colorectal Cancer. *J Clin Oncol* **26**, 3213–3221 (2008).
27. Harouaka, R. A., Nisic, M. & Zheng, S.-Y. Circulating Tumor Cell Enrichment Based on Physical Properties. *J Lab Autom* **18**, 455–468 (2013).
28. Shim, S. et al. Antibody-independent isolation of circulating tumor cells by continuous-flow dielectrophoresis. *Biomicrofluidics* **7**, 011807, 1–12 (2013).
29. Baccelli, I. et al. Identification of a population of blood circulating tumor cells from breast cancer patients that initiates metastasis in a xenograft assay. *Nat Biotech* **31**, 539–544 (2013).
30. Fischer, J. C. et al. Diagnostic leukapheresis enables reliable detection of circulating tumor cells of nonmetastatic cancer patients. *Proc Natl Acad Sci* **110**, 16580–16855 (2013).
31. Sollier, E. et al. Size-selective collection of circulating tumor cells using Vortex technology. *Lab Chip* **14**, 63–77 (2014).
32. Samlowski, W. E., McGregor, J. R., Tharkar, S., Donepudi, S. & Ferrone, S. Isolation and Expansion of Circulating Tumor Cells (CTC) from Melanoma Patients Using a Novel Cell Culture Technique. *J Clin Oncol* **30**, abstr 10614 (2012).
33. Donepudi, S. et al. Circulating Tumor Cell Cultures as a Predictive Marker during Salvage Therapy of Refractory Merkel Cell Carcinoma with Chemotherapy and Electron Beam Radiation. *JCT* **4**, 1162–1166 (2013).
34. Zhang, L. et al. The Identification and Characterization of Breast Cancer CTCs Competent for Brain Metastasis. *Sci Transl Med* **5**, 180ra148 (2013).
35. Kirby, B. J. et al. Functional Characterization of Circulating Tumor Cells with a Prostate-Cancer-Specific Microfluidic Device. *PLoS ONE* **7**, e35976, 1–10 (2012).
36. Zheng, S. et al. Membrane microfilter device for selective capture, electrolysis and genomic analysis of human circulating tumor cells. *J Chromatogr* **1162**, 154–161 (2007).
37. Zheng, S. et al. 3D microfilter device for viable circulating tumor cell (CTC) enrichment from blood. *Biomed Microdevices* **13**, 203–213 (2011).
38. Harouaka, R. A. et al. Flexible micro spring array device for high-throughput enrichment of viable circulating tumor cells. *Clin Chem* **60**, 323–333 (2014).
39. Kojima, T. et al. A simple biological imaging system for detecting viable human circulating tumor cells. *JCI* **119**, 3172–3181 (2009).
40. Pulaski, B. A. & Ostrand-Rosenberg, S. in *Curr Protoc Immunol* (John Wiley & Sons, Inc., Hoboken, NJ, 2001).
41. Königsberg, R. et al. Detection of EpCAM positive and negative circulating tumor cells in metastatic breast cancer patients. *Acta Oncol* **50**, 700–710 (2011).
42. Attard, G. & de Bono, J. S. Utilizing circulating tumor cells: challenges and pitfalls. *Curr Opin Genet Dev* **21**, 50–58 (2011).
43. Went, P. T. H. et al. Frequent EpCam protein expression in human carcinomas. *Hum Pathol* **35**, 122–128 (2004).
44. Rao, C. G. et al. Expression of epithelial cell adhesion molecule in carcinoma cells present in blood and primary and metastatic tumors. *Int J Oncol* **27**, 49–57 (2005).
45. Fleischer, R. L., Price, P. B. & Symes, E. M. Novel Filter for Biological Materials. *Science* **143**, 249–250 (1964).
46. Lin, H. K. et al. Portable filter-based microdevice for detection and characterization of circulating tumor cells. *Clin Cancer Res* **16**, 5011–5018 (2010).
47. Wolfensohn, S. & Lloyd, M. *Handbook of Laboratory Animal Management and Welfare, 4th Edition.* (Wiley-Blackwell, Hoboken, NJ, 2013).
48. Yu, M. et al. Ex vivo culture of circulating breast tumor cells for individualized testing of drug susceptibility. *Science* **345**, 216–220 (2014).
49. Ince, T. A. et al. Transformation of Different Human Breast Epithelial Cell Types Leads to Distinct Tumor Phenotypes. *Cancer Cell* **12**, 160–170 (2007).
50. Liu, X. et al. ROCK Inhibitor and Feeder Cells Induce the Conditional Reprogramming of Epithelial Cells. *Am J Pathol* **180**, 599–607 (2012).

51. Yuan, H. *et al.* Use of Reprogrammed Cells to Identify Therapy for Respiratory Papillomatosis. *NEJM* **367**, 1220–1227 (2012).

Acknowledgments

Author contributions

M.-D.Z. designed, fabricated, optimized the device. S.H. performed in vitro device characterization, clinical sample testing, and data analysis. A.W. performed animal model experiments and related data analysis. R.H. constructed of the flow control system and provided technical support of in vitro device characterization and clinical sample testing. B.S., R.B. and E.G. provided animal model system design and technical support for animal model system. S.R. and Z.A. provided technical Support for viable CTC capture and culture and performed data analysis. B.L. performed on-chip cell culture of multiple cell lines on device. S.W. and J.Z. designed, constructed and characterized the virus used for the on-chip cell viability assay. R.D. and R.C. provided project mentoring and animal model system design. Y.-C.T. contributed to the initial device concept and design, and provided project mentoring. S.-Y.Z. provided overall project mentoring, contribute to device concept, design, fabrication process development, experimental design, and data analysis. S.-Y.Z., S.H. and A.W. wrote the manuscript.

Additional information

CORRIGENDUM: Separable Bilayer Microfiltration Device for Viable Label-free Enrichment of Circulating Tumour Cells

Ming-Da Zhou, Sijie Hao, Anthony J. Williams, Ramdane A. Harouaka, Brett Schrand, Siddarth Rawal, Zheng Ao, Randall Brenneman, Eli Gilboa, Bo Lu, Shuwen Wang, Jiyue Zhu, Ram Datar, Richard Cote, Yu-Chong Tai & Si-Yang Zheng

The original version of this Article contained a typographical error in the spelling of the author Randall Brenneman which was incorrectly given as Randall Brennaman. This has now been corrected in the PDF and HTML versions of the Article.